Geochemistry, Geophysics, Geosystems

RESEARCH ARTICLE
10.1029/2020GC009108

Key Points:
- Two consistent thermal conductivity profiles were obtained down to ~3 km below the seafloor in the Nankai Trough accretionary prism
- We pressurized shallow overlying sediments on an oceanic plate to simulate deeper sediments in an accretionary prism by reducing porosity
- We obtained an empirical thermal conductivity-porosity relation for Nankai Trough sediments applicable to a basin and accretionary prism

Correspondence to:
W. Lin,
lin@kumst.kyoto-u.ac.jp

Citation:
Lin, W., Hirose, T., Tadai, O., Tanikawa, W., Ishitsuka, K., & Yang, X. (2020). Thermal conductivity profile in the Nankai accretionary prism at IODP NanTroSEIZE Site C0002: Estimations from high-pressure experiments using input site sediments. *Geochemistry, Geophysics, Geosystems*, *21*, e2020GC009108. https://doi.org/10.1029/2020GC009108

Received 15 APR 2020
Accepted 25 JUN 2020
Accepted article online 30 JUN 2020

Thermal Conductivity Profile in the Nankai Accretionary Prism at IODP NanTroSEIZE Site C0002: Estimations From High-Pressure Experiments Using Input Site Sediments

Weiren Lin[1], Takehiro Hirose[2], Osamu Tadai[3], Wataru Tanikawa[2], Kazuya Ishitsuka[1], and Xiaoqiu Yang[4,5]

[1]Graduate School of Engineering, Kyoto University, Kyoto, Japan, [2]Japan Agency for Marine-Earth Science and Technology (JAMSTEC), Kochi Institute for Core Sample Research, X-star, Nankoku, Japan, [3]Marine Works Japan LTD, Nankoku, Japan, [4]Key Laboratory of Ocean and Marginal Sea Geology, South China Sea Institute of Oceanology, Innovation Academy of South China Sea Ecology and Environmental Engineering, Chinese Academy of Sciences, Guangzhou, China, [5]Southern Marine Science and Engineering Guangdong Laboratory (Guangzhou), Guangzhou, China

Abstract Depth profiles of sediment thermal conductivity are required for understanding the thermal structure in active seismogenic zones. During the Nankai Trough Seismogenic Zone Experiment (NanTroSEIZE), a scientific drilling project of the International Ocean Discovery Program (IODP), a borehole was penetrated to a depth of 3,262.5 m below seafloor (mbsf) at Site C0002. Because core samples obtained from below ~1,100 mbsf in an accretionary prism are limited, a thermal conductivity profile over such depths usually determined by laboratory measurements using core samples is not available. To obtain the thermal conductivity profile at Site C0002, we used core samples collected from sediments that overlay the incoming subducting oceanic basement at Nankai Trough Seismogenic Zone Experiment Site C0012, which can be considered to have the same mineral composition as the accretional prism at Site C0002. The thermal conductivity of the C0012 core samples was measured at high pressure to simulate subduction by reducing the sample porosity. We measured the thermal conductivity of six core samples from 144–518 mbsf at Site C0012 up to a maximum effective pressure of ~50 MPa, corresponding to depths greater than ~4 km below seafloor. We obtained an empirical relation between thermal conductivity λ_{Bulk} in $Wm^{-1}K^{-1}$ and fractional porosity ϕ for the Nankai Trough accretionary prism as $\lambda_{Bulk} = \exp(-1.09\phi + 0.977)$. Based on porosity data measured using core/cuttings samples and data derived from *P* wave velocity logs, we estimate two consistent and complete thermal conductivity profiles down to ~3 km below seafloor in the Nankai Trough accretionary prism. These profiles are consistent with the existing thermal conductivity data measured using limited core samples.

Plain Language Summary Depth profiles of sediment thermal conductivity are required for understanding the thermal structure and earthquake occurrences in active seismogenic zones such as the Nankai Trough, SW Japan. The depth profile in Nankai Trough accretionary prism, however, is not available because sediment drill core samples from great depths are hard to be obtained. We collected six core samples from shallower sediments that overlay the incoming subducting oceanic basement at Nankai Trough Drill Site C0012 by IODP, which can be considered to have the same solid grain components as the accretional prism at Site C0002. The thermal conductivity of the C0012 core samples was measured at high pressure. We pressurized the core samples to simulate deeper sediments in accretionary prism by reducing sample porosity. As the result, we obtained an empirical relation between thermal conductivity and porosity for the Nankai Trough sediments and then estimated thermal conductivity profiles down to ~3 km below seafloor based on porosity profiles in the Nankai Trough accretionary prism.

1. Introduction

The Nankai convergent subduction zone in southwest Japan is one of the most active seismogenic zones in the world, where megathrust earthquakes (Mw > 8) have occurred over recurrence intervals of 100–200 years (Ando, 1975), which are shorter than other main seismogenic subduction zones. For a comprehensive understanding of this seismogenic zone, the International Ocean Discovery Program (IODP, known as the

Integrated Ocean Drilling Program before 2013) conducted 13 expeditions as part of the Nankai Trough Seismogenic Zone Experiment (NanTroSEIZE) project from 2007 to 2019 (Kinoshita et al., 2006; Tobin, Hirose, et al., 2019). The NanTroSEIZE is a multidisciplinary investigation of fault mechanics and seismogenesis along subduction megathrusts and includes reflection and refraction seismic imaging, direct sampling by drilling, in situ measurements, and long-term monitoring in conjunction with laboratory and numerical modeling studies (Tobin, Kimura, & Kodaira, 2019).

Temperature plays a key role in seismogenesis at subduction zones and is thought to govern the nature of slip along active subduction thrusts, as well as the upper and lower transitions of seismogenic zones (e.g., Harris & Wang, 2002; Hyndman et al., 1995; Wang et al., 1995; Yamano et al., 2003). Specifically, temperature controls the rupturing properties of fault materials (e.g., slip velocity dependence of the frictional coefficient), pore fluid transportation properties that affect pore fluid pressure and thus fault strength, and water-rock reactions that affect fault strength recovery (e.g., Mizutani et al., 2017; Scholz, 1998; Stesky et al., 1974; Tanikawa et al., 2013). Conversely, thermal conductivity also controls the coseismic temperature that increases in and around fault slip zones caused by frictional heating and affects the postseismic diffusion process of frictional heating and temperature recovery processes (e.g., Fulton et al., 2013).

Depth profiles of the thermal conductivity of sediments in accretionary prisms in subduction zones are necessary and important for understanding the temperature structure and heat flow around a megathrust (Harris et al., 2011; Spinelli, 2014; Tanikawa et al., 2016). At the centerpiece Site C0002 of the NanTroSEIZE, a borehole was penetrated to a depth of 3,262.5 m below seafloor (mbsf), which is the deepest of all the scientific ocean drilling programs (Tobin, Hirose, et al., 2019). However, a very limited number of core samples were collected below ~1,100 mbsf at Site C0002, which is located in the accretionary prism above the seismogenic zone. Consequently, available thermal conductivity data remain limited in the accretionary prism because thermal conductivity measurements require core samples. Fortunately, a complete porosity depth profile is available from laboratory measurements using continuously recovered cuttings samples. A porosity depth profile can also be derived from *P* wave velocities and/or resistivity logs. The problem is therefore how to reasonably establish the relationship between the thermal conductivity and porosity of the sediments in the accretionary prism of Site C0002.

IODP Expeditions 322 and 333 of the NanTroSEIZE project drilled at Input Sites C0011 and C0012, which are on the Philippine Sea plate and will eventually be subducted beneath the Eurasian plate (Figures 1 and 2; Underwood et al., 2010; Expedition 333 Scientists, 2012a). The overlaying sediments at the input site will be transported to the underthrust strata and/or accrete to the accretionary prism above the plate boundary fault (décollement; Figure 2). The sediment core samples recovered at an input site therefore allow estimation of the thermal conductivity of the accretionary prism because sediments from both the input site and accretionary prism are expected to have the same or similar solid grain components. Expedition reports used X-ray diffraction analysis to confirm that the major mineral composition of sediments (clay minerals, quartz, feldspar, and calcite) is the same at Input Site C0012 as the accretionary prism down to 3,058.5 mbsf at Site C0002 (Expedition 322 Scientists, 2012a; Expedition 333 Scientists, 2012b; Tobin et al., 2015b). The thermal conductivity of the sediments will also change during subduction because compaction will decrease their porosity with depth. The relationship between thermal conductivity changes and porosity reductions caused by increased pressure should therefore be simulated in laboratory measurements using core samples from shallow input sites. This relationship allows estimations of thermal conductivity of the deeper accretionary prism once the porosity is obtained.

Many previous studies have measured the thermal conductivity of hard rocks at high pressure, even up to pressures above 1 GPa (e.g., Abdulagatova et al., 2009; Horai & Susaki, 1989; Kukkonen et al., 1999; Osako et al., 2004; Pribnow et al., 1996; Seipold & Huenges, 1998; Xu et al., 2004), but only a few measurements from ocean sediments have been reported (e.g., Lin et al., 2011; Morin & Silva, 1984). There is no systematic data set in the literatures of the effect of pressure on the thermal conductivity of subduction zone sediments for simulating subduction. Furthermore, no experimental data have been published on the effects of pressure on the thermal conductivity of sediments from the Nankai Trough region except for our preliminary findings (Lin et al., 2011).

In this study, we measured the thermal conductivity of six core samples from sediments overlaying the subducting Philippine Sea plate under conditions of high confining and pore fluid pressures and monitored the

10.1029/2020GC009108

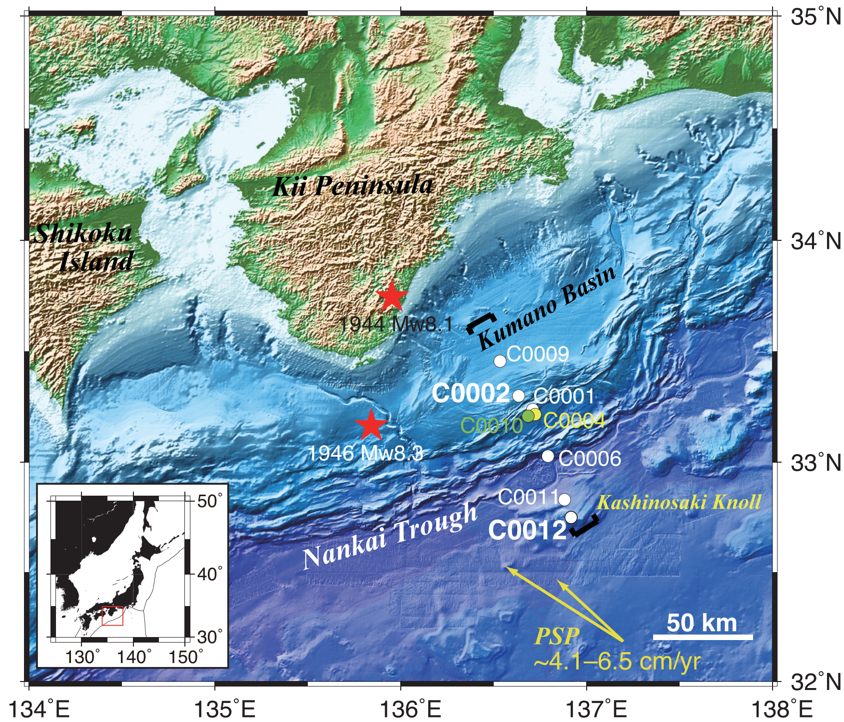

Figure 1. Topographic map of the NanTroSEIZE study area (modified from Lin et al., 2016). Two red stars show the epicenters of the 1944 Tonankai and 1946 Nankai earthquakes. The circles and labels (e.g., C0012) show the locations of NanTroSEIZE drilling sites. PSP denotes the Philippine Sea Plate, and the yellow arrows show the far-field convergence vectors between the Philippine Sea plate and Japan (Heki & Miyazaki, 2001; Miyazaki & Heki, 2001). Brackets show location of the cross–section in Figure 2. The red rectangle in the inset shows the location of the main map.

porosity changes of the test samples. The thermal conductivity changes of the sediments were examined over a wide porosity range from ~60% to ~20%, which matches the porosity of the accretionary prism down to ~3 km below the seafloor (kmbsf) and approximately corresponds to the current hole bottom at NanTroSEIZE Site C0002. On the basis of this data set, we established an empirical equation that describes the relationship between thermal conductivity and porosity of the sediments. We then estimated thermal conductivity depth profiles of the accretionary prism above the Nankai seismogenic zone based on the porosity data.

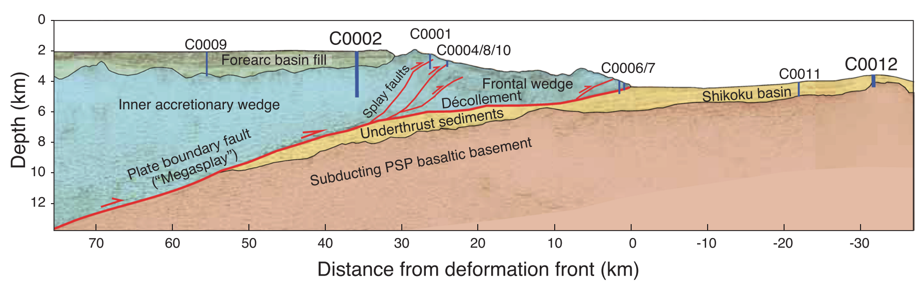

Figure 2. Seismic reflection depth section with tectonic interpretation of the NanTroSEIZE transect, originally published by Park et al. (2002) as Section Line 5 (modified from Tobin et al., 2015a). Depth denotes the depth below sea level. PSP denotes the Philippine Sea plate. The sediment core samples used in this study were retrieved from Input Site C0012.

2. Tectonic Setting and Experimental Samples

2.1. Nankai Subduction Zone and NanTroSEIZE

The Nankai Trough region in southwest Japan is one of the most extensively studied subduction zones in the world (e.g., Yamamoto et al., 2013). The subducting Philippine Sea plate is currently moving northwest beneath the Eurasian plate at a rate of ~4–6 cm/year (Heki & Miyazaki, 2001; Miyazaki & Heki, 2001; Seno et al., 1993), roughly orthogonal to the axis of the Nankai Trough (Figure 1). In this area, M_w 8.0 class earthquakes occur frequently because of the convergence of the Philippine Sea and Eurasian plates. The last two great earthquakes in the Nankai subduction zone occurred in 1944 (Tonankai, M 8.0–8.3) and 1946 (Nankai, M 8.1–8.4), generating tsunamis and causing significant damage in southwestern Japan (Kanamori, 1972). The updip limit of the Nankai Trough seismogenic zone (i.e., locked zone of the plate boundary fault) is up to ~5 kmbsf and considered accessible by the riser drilling vessel *D/V Chikyu*. The NanTroSEIZE project was designed to investigate the mechanics of the subduction megathrust from drilling and a wide range of related studies (Tobin, Kimura, & Kodaira, 2019; Tobin & Kinoshita, 2006). A challenging plan was established to drill through the seismogenic zone to a depth of ~5 kmbsf at Site C0002, where the updip limit of the coseismic slip zone of the 1944 Tonankai earthquake is located (Figures 1 and 2). The drilling operations of NanTroSEIZE were performed in multiple expeditions since 2007 as IODP Expeditions 314 and 315. A penetration depth of 3,262.5 mbsf was achieved in the fourth stage of Expedition 358 and will probably be retried in the future (Tobin, Hirose, et al., 2019; Tobin, Kimura, & Kodaira, 2019). Conversely, IODP Expeditions 322 and 333 were designed to drill on the incoming Philippine Sea plate at two reference sites called "input sites" that included Site C0012 and sampled materials including overlaying sediments and basaltic basement (Figures 1 and 2) (Saito et al., 2009). The basement will ultimately subduct into deeper oceanic crust, but the sediments will become the underthrust sediments and/or accrete onto the accretionary prism. They will then compose the seismogenic zone around the plate boundary interface in the future. Site C0012 is located ~31 km seaward of the trench on a basement high (the Kashino knoll) and includes samples of a condensed section from shallow sedimentary rocks to basaltic basement (Expedition 333 Scientists, 2012a; Underwood et al., 2010).

2.2. Core Samples

To estimate the thermal conductivity of the accretionary prism of the Nankai Trough subduction zone (i.e., below the unconformity at ~922 mbsf at Site C0002), we collected six sediment core samples that cover all of the lithological units from Hole C0012A drilled during Expedition 322 in 2009 and C0012D and C0012G during Expedition 333 in 2011 at almost the same location (32°44.9′N, 136°55.0′E) (Expedition 322 Scientists, 2012a; Expedition 333 Scientists, 2012b). The sediment core samples were taken from a depth range of 144–518 mbsf, and the boundary between overlying sediments and basaltic basement was documented at ~526 mbsf. The water depth at the borehole locations is ~3,500 m. The wet bulk density (bulk density of water saturated samples), grain density, porosity, and thermal conductivity of the sediment core samples were measured in the laboratory under atmospheric pressure and room temperature conditions (Table 1). These fundamental physical properties are in good agreement with onboard measurement results (Expedition 333 Scientists, 2012b). Wet bulk density and porosity were determined using the buoyancy method, in which the sample was dried at ~110°C (Franklin, 1979).

Multiple boreholes were penetrated at Site C0012 during multiexpeditions to achieve good quality core samples and completely cover all of the sediments and basaltic basement. From the seafloor to the bottom of the overlaying sediments, the formations are divided into six units. These include units: (I) upper Shikoku basin facies (above ~150 mbsf, hemipelagic deposits, late Miocene to early Pliocene), (II) middle Shikoku basin facies (~150–220 mbsf, hemipelagic deposits, late Miocene), (III) lower Shikoku basin hemipelagic facies (~220–332 mbsf, hemipelagic deposits, middle to late Miocene), (IV) lower Shikoku basin turbidite facies (~332–416 mbsf, hemipelagic deposits and silty turbidity currents, middle Miocene), (V) volcaniclastic-rich facies (~416–528 mbsf in C0012A, hemipelagic deposits, volcaniclastic turbidity currents, etc., mainly middle Miocene), and (VI) pelagic clay facies (~500–526 mbsf in C0012G, pelagic deposits including reddish brown calcareous claystone, early Miocene) (Expedition 322 Scientists, 2010a; Expedition 333 Scientists, 2012b). We retrieved one core for each lithological unit mentioned above, and the lithology at each depth of the core samples is listed in Table 1. We used the six hemipelagic and pelagic

Table 1
Sample ID, Depth, Lithological Unit, Lithology, Geological Age, and Basic Physical Properties

Sample ID[a]	Depth (mbsf)	Lithological unit, lithology, and age	Wet bulk density (kg/m^3)	Grain density (kg/m^3)	Porosity (%)	Thermal conductivity[b] (Wm^{-1} K^{-1})
C0012D05H3	~144	Unit IC, hemipelagic mud, late Miocene	1,710	2,790	60.6	1.34 ± 0.02
C0012A19R1	~217	Unit II, siltstone, middle Miocene	1,840	2,790	53.4	1.48 ± 0.01
C0012A23R6	~259	Unit III, hemipelagic mudstone, middle Miocene	1,880	2,790	50.9	1.47 ± 0.01
C0012A32R3	~341	Unit IV, hemipelagic mudstone, middle Miocene	1,940	2,790	47.2	1.52 ± 0.03
C0012A43R2	~445	Unit V, hemipelagic mudstone, middle Miocene	2,040	2,710	39.5	1.50 ± 0.03
C0012G01R4	~518	Unit VI, calcareous pelagic claystone, early Miocene	2,230	2,860	33.8	1.80 ± 0.07
C0012G07RCC	~573	Unit VII, basalt, early Miocene	2,570	2,810	3.9–8.7[c]	1.70 ± 0.01

Note. Density and porosity under atmospheric pressure were determined by the buoyancy method (Franklin, 1979). Lithology and age data are after Expedition 322 Scientists (2010a) and Expedition 333 Scientists (2012b). The physical properties of C0012G07RCC are after Lin et al. (2018).
[a]The Core Sample Name C0012A19R1 denotes that it was retrieved from the Site C0012, Borehole A, nineteenth rotary-drilled core, first core section. In addition, "H" of C0012D05H3 means hydraulic piston coring system (HPCS), and "CC" of C0012G07RCC is from the core catcher. [b]Thermal conductivity was measured in this study under atmospheric pressure and room temperature conditions. [c]The corrected measured porosity was estimated as in the range by Lin et al. (2018).

sediment core samples to measure thermal conductivity under high confining and pore fluid pressures and room temperature.

3. Experimental Protocol

In our previous study (Lin et al., 2011), we established a thermal conductivity measurement system for rock samples under high confining pressure but without pore pressure control. The first data set used two soft sediment core samples from Site C0001 of NanTroSEIZE and hard rocks including fresh granites from terrestrial quarries to demonstrate that the measurement methods are effective for examining the effects of high confining pressure on the thermal conductivity of core samples (Lin et al., 2011). For a more exact simulation of not only lithostatic pressure but also pore fluid pressure, we developed a system with a pore pressure control function. This system can monitor pore water drainage and sample deformation under high pressure and enables the estimation of porosity changes under high-pressure conditions. The apparatus comprises two highly accurate pressure controlling syringe pumps (Teledyne Isco, 260D and 65D; https://store.teledyneisco.com/) used for controlling the confining and pore pressure and monitoring both pressure and flow volume (Figure 3). This system was first used for thermal conductivity measurements using basaltic samples including a core sample from the same Site C0012. For the thermal conductivity measurements, we used the same thermal conductivity meter, QTM-500 (Kyoto Electronics Manufacturing, Kyoto, Japan; https://www.kyoto%2010kem.com/en/), as that of Lin et al. (2011), which is based on transient heating of a half-space sample by a line source (Galson et al., 1987; Sass et al., 1984). We also used the same line-source sensor probe in the high-pressure vessel and data analyses designed and created in the previous study, as well as the same sample assembly as Lin et al. (2011) and Lin et al. (2018) (Figure 4). The rock samples were half cylinders with an ~5-cm diameter and ~10-cm length.

For thermal conductivity measurements using the transient line-source devices of the QTM-500, lower thermal conductivities of the test sample were associated with steeper temperature increases during heating (Lin et al., 2011). In principle, the temperature should increase linearly on a semilogarithmic scale between temperature and heating time after a certain initial time. During our high-pressure measurements, the temperature curves show a nearly linear increasing pattern in a time range from 20 to 60 s in which the temperature increase gradient was calculated (Figure 5). The gradient decreases with increasing effective pressure, indicating that the apparent thermal conductivity of the rock and Teflon pair increases with increasing effective pressure.

Because the axial direction of the core samples was oriented vertically, the measured thermal conductivity reflects that in the horizontal direction in its in situ position. Similar to orderly deposited ocean

10.1029/2020GC009108

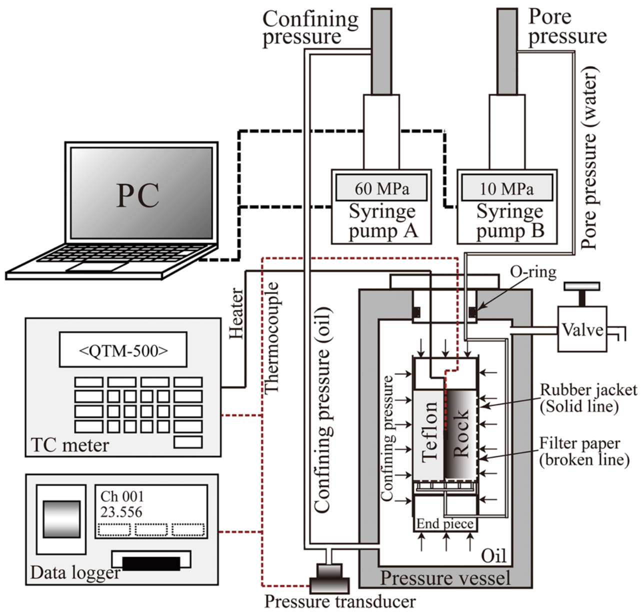

Figure 3. Schematic diagram of the apparatus used in this study (modified from Lin et al., 2018) for thermal conductivity measurements under high confining pressure and high pore pressure conditions. The system comprises a hydrostatic pressure vessel with two servo-controlled syringe pumps, a wire-type line-source sensor in the pressure vessel, a thermal-conductivity meter (QTM-500) to measure thermal conductivity from the wire sensor, and a data logger. One syringe pump provides high pressures up to ~138 MPa for confining pressure and the other up to ~52 MPa for pore pressure. The pore pressure pump monitors the drained water volume to calculate the change in total pore volume of the water-saturated rock samples associated with sample deformation.

sediments, Lin et al. (2014) showed that the thermal conductivity anisotropy of core samples collected from Japan Trench Drilling Site C0019 above the plate interface was less than ~3%, which is almost the same as the thermal conductivity precision.

To simulate subduction of the overlaying sediments, we increased the confining pressure stepwise to 60 MPa while holding the pore pressure constant at 10 MPa. We then measured the thermal conductivity at each confining pressure. We define the effective pressure P_{eff} as the difference of confining pressure P_c and pore pressure P_p, that is, $P_{\text{eff}} = P_c - P_p$. We set the effective pressures of the thermal conductivity measurements to 1, 5, 10, 20, 30, 40, and 50 MPa (Figure 6a). Because all of the sediment core samples used in this study were retrieved from relatively shallow depths (<518 mbsf), effective pressures greater than 5 MPa exceed the maximum pressure the rock of the core sample had experienced. The high pressures thus caused larger deformation, called normal consolidation, and sometimes broke the sealing rubber jacket, after which confining pressure medium (oil) entered the inside of the sample assembly.

4. Results

4.1. Thermal Conductivity Under High Confining and Pore Pressure Conditions

Figure 6 shows a typical thermal conductivity measurement of Core Sample C0012A19R1 retrieved from ~217 mbsf at Site C0012. As a rough estimation from its depth, the maximum effective pressure that the core sample had previously experienced might have been ~2 MPa. We loaded the confining pressure to ~1.5 MPa and pore pressure to ~0.5 MPa (effective pressure of ~1.0 MPa) for 1 day and then to ~11 and ~10 MPa, respectively, for 1 day in the second step (Figure 6a). The confining pressure was then increased stepwise to ~12, 15, 20, and 30 MPa, but the pore pressure was maintained at ~10 MPa. A few hours after loading to ~30 MPa, the rubber jacket broke, and the experiment was terminated after a total of ~43 days.

During the pressure loading and maintenance, water drainage was monitored by a 260D syringe pump used for pore pressure control. The following assumptions were made: (a) water intake and output are equal to total pore volume change, and (b) the initial porosity of the test sample at the beginning of the experiment is the same as that measured by the buoyancy method using a neighboring subsample cut from the thermal conductivity test sample (53.4%; Table 1). The estimated porosity $\phi(t)$ at an arbitrary elapsed time t was determined using

$$\phi(t) = (V_{\text{WI}} - V_{\text{Drain}}(t))/(V_{\text{SI}} - V_{\text{Drain}}(t)), \tag{1}$$

where V_{SI} is the initial sample volume, V_{WI} is the initial pore volume of the sample saturated by water, and $V_{\text{Drain}}(t)$ is the volume of water drained at an arbitrary time assumed to be equal to the change of pore volume relative to the initial volume. The pore volume at a given time was calculated by subtracting $V_{\text{Drain}}(t)$ measured by the 260D pump from V_{WI}. The sample volume at a given time was calculated by subtracting its volumetric change assumed to be equal to the pore volume change as $V_{\text{SI}} - V_{\text{Drain}}(t)$. Because the sample assembly and steel tubes for pore fluids in the pressure vessel were deformed during the confining pressure change, we calibrated the system deformation and corrected the raw pump data of water drainage to obtain $V_{\text{Drain}}(t)$ for estimating porosity changes in the same way as described in Lin et al. (2018).

The estimated porosity of Sample C0012A19R1 is shown in Figure 6b as a function of elapsed time. During the first loading step, the porosity of the core sample decreased by ~2%, possibly caused by a porosity increase

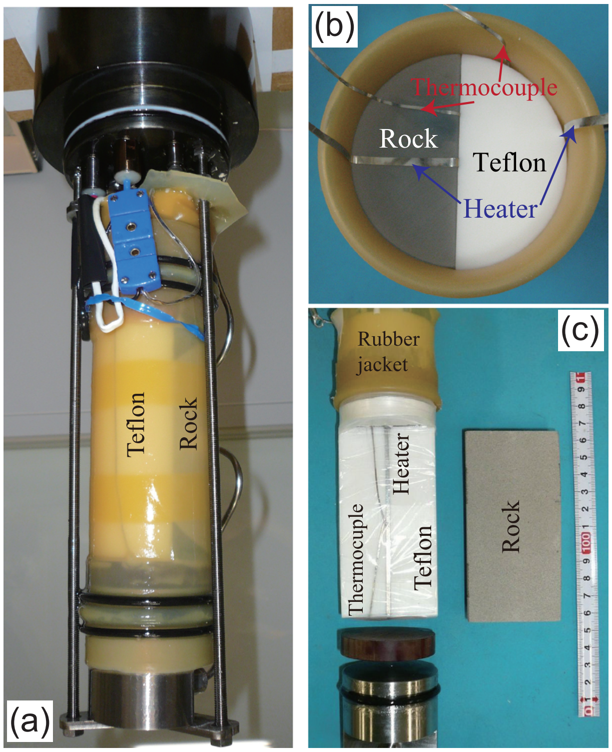

Figure 4. Photos of the sample assembly for thermal conductivity measurements under high confining and pore fluid pressures. (a) Assembly of a half-cylindrical rock sample and a Teflon piece of the same shape and size. (b) Top view of the rock sample and Teflon. (c) Prior to set up.

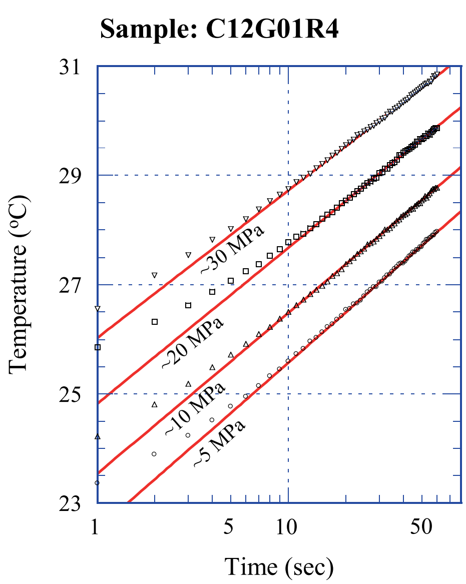

Figure 5. Examples of thermal conductivity measurements for Sediment Core Sample C0012G0104 at four different confining pressures. The gradient in a time range from 20 to 60 s of each data set in semilogarithmic scale is inversely proportional to thermal conductivity. Labels beside the data plots indicate the effective pressure ($P_{\mathrm{eff}} = P_{\mathrm{c}} - P_{\mathrm{p}}$).

owing to rebound accompanied with the in situ stress relief by drilling. This decrease may also have some uncertainty owing to air in the sample assembly and experimental system prior to pressurizing. At effective pressure conditions of ~2 MPa or lower, the estimated porosity does not substantially decrease because the sample had already undergone such pressures prior to retrieval from its in situ depth. However, once the effective pressure conditions (5 and/or 10 MPa) exceed a certain level (~2 MPa) that the sample had previously experienced, its porosity gradually and then significantly decreases. Moreover, the porosity reduction process (consolidation) continues over a long time duration. For example, the porosity decrease did not completely stabilize even ~30 days after pressurization to 20 MPa confining pressure. As a result, the porosity of this sample loaded to an effective pressure 10 MPa decreased by ~15% over ~43 days.

The thermal conductivity was measured multiple times at each pressure condition ("+" symbols in Figure 6a represent measuring points) in cases that the pressure condition was held for more than 1 day, amounting to an average of one measurement per day on weekdays. Thermal conductivity measurements were repeated six or seven times at each measuring point. The measured values show a small degree of scatter with a relative standard deviation of <3%, as shown in Figure 6c where measured values and their mean are represented by blue squares and red circles, respectively. The full thermal conductivity data set measured from the six sediment core samples is stored and provided in a data repository (https://doi.pangaea.de/10.1594/PANGAEA.914950).

The results of Sample C0012A19R1 show that thermal conductivity increases not only with effective pressure but also over elapsed time or when porosity decreases even under the same effective pressure condition (Figures 6b and 6c). We also measured thermal conductivity after termination of the experiment on the 42nd day and one more time on the 43rd day under atmospheric pressure conditions. Surprisingly, the results show a lower thermal conductivity on the 43rd day than the 42nd day (Figure 6c). This may reflect time-dependent strain recovery caused by the pressure relief. Byrne et al. (2009), Yamamoto et al. (2013), and Oohashi et al. (2017) successfully applied this strain-recovery principle to constrain the three-dimensional in situ stress state of the NanTroSEIZE project.

4.2. Thermal Conductivity Changes With Increasing Pressure and Decreasing Porosity

Figure 7 shows thermal conductivity values measured at various effective pressure conditions for all the six sediment samples in this study and the basalt sample (C0012G07RCC) after Lin et al. (2018). Thermal conductivity was also measured under atmospheric pressure conditions prior to increasing the confining and pore pressure. The results show that thermal conductivity generally increases with depth (Table 1) but appears to depend on the sample lithology and detailed mineral composition. Overall, the thermal conductivity of wet core samples (seawater saturated) increases with increasing effective pressure (Figure 7). As mentioned, as the consolidation process progresses (i.e., decrease of sample porosity), thermal

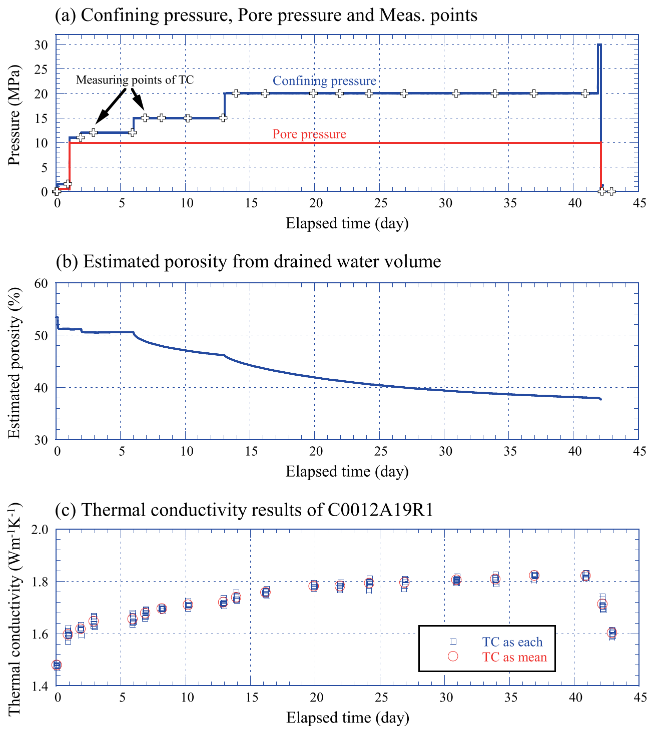

Figure 6. The data set of thermal conductivity measurements for Sediment Core Sample C0012A19R1: (a) real data of confining and pore pressures and measurement points of thermal conductivity, (b) estimated porosity, and (c) thermal conductivity results. The porosity under high pressure was estimated from the porosity under atmospheric pressure (initial porosity) and pore volume change detected by the pore water drainage. We increased the confining pressure stepwise to simulate subsidence and compaction and held the pore pressure constant at 10 MPa except for the first and last steps of the test. While keeping the pressure constant, the pore water drainage progressed, but its rate gradually decreased. The symbol "+" in (a) indicates the time points at which thermal conductivity measurements were collected. This test lasted ~43 days with accurate pressure control by the pumps over this duration.

conductivity increases even under the same effective pressure conditions (Figure 7b).

In the light of the observation that the thermal conductivity of a sediment core sample is more directly and strongly dependent on porosity than effective pressure conditions, we show the relationship between measured thermal conductivity and porosity estimated from the drained water volume of the six sediment core samples in Figure 8a. A clear trend is observed for all of the samples in which the thermal conductivity increases with decreasing porosity. Although the detailed curves differed between samples owing to differences in lithology and mineral composition, for example, Core Sample C0012A19R1 shows higher thermal conductivities than the others, the relationship between thermal conductivity and porosity is essentially the same. In the lower part of the Lithologic Unit II of Site C0012 where C0012A19R1 is located, lithologies appear as consolidated volcanic sandstone turbidites, including fresh and altered glass with some associated calcite (Expedition 333 Scientists, 2012b). Smear slide observations of C0012A19R4 from the same core as C0012A19R1 showed that the lithology of this core is sandstone, consisting of sand ~75%, silt ~15%, and clay ~10%, and much different with the others (Expedition 322 Scientists, 2010b). Probably, these features brought the measurement results of higher thermal conductivities for C0012A19R1.

In sedimentary rocks, there are several well-known relationships, called the mixing laws, for example, the geometric mean and square root mean usually applied to randomly oriented and distributed grains in a mixture, harmonic mean to beds layered perpendicular to the direction of heat flow, and arithmetic mean to beds arranged parallel to heat flow direction (Beardsmore & Cull, 2001). Fuchs et al. (2013) evaluated five common mixing laws including the geometric, arithmetic, and harmonic means for calculating bulk thermal conductivity of sedimentary rocks and concluded that the geometric mean displays the best. As the geometric mean, relationship between

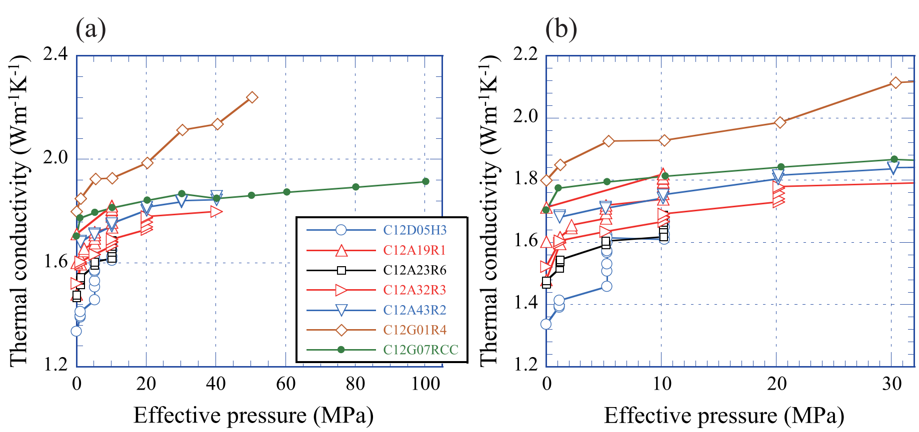

Figure 7. Relationships between measured thermal conductivity and effective pressure of the six sediment core samples alongside a basalt sample (C12G07RCC) after Lin et al. (2018). (a) and (b) show the same data but in different effective pressure ranges. We measured the thermal conductivity six or seven times at each point (see "+" in Figure 6a). The data points in these figures represent the mean values of the measured thermal conductivities. Porosity estimation for the Core Sample C12G01R4 under effective pressure 50 MPa was failed due to a leak of a tube joint of pore water controlling, consequently the thermal conductivity data cannot be plotted in Figure 8.

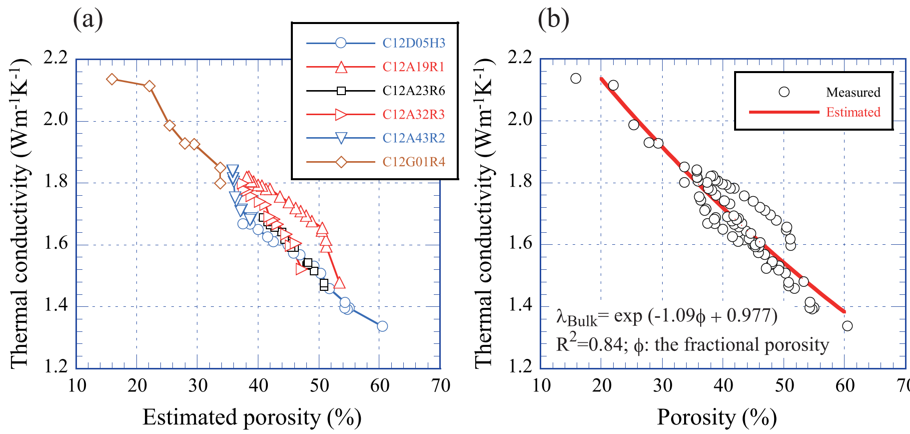

Figure 8. Relationships between measured thermal conductivity and estimated porosity of the six sediment core samples: (a) as individual samples and (b) as all of the six samples. The red curve shows a logarithmic regression line based on all of the data except the basalt (C12G07RCC). As in Figure 7, each plot shows the mean value of the measured thermal conductivities at the same time point.

bulk thermal conductivity of a rock sample in a water saturated state and porosity is as follows:

$$\lambda_{\text{Bulk}} = \lambda_{\text{Water}}{}^{\phi}\, \lambda_{\text{Grain}}{}^{(1-\phi)}, \tag{2}$$

or

$$\ln\left(\lambda_{\text{Bulk}}\right) = \phi \ln\left(\lambda_{\text{Water}}/\lambda_{\text{Grain}}\right) + \ln\left(\lambda_{\text{Grain}}\right), \tag{3}$$

where λ_{Bulk} is the bulk thermal conductivity of a water-saturated rock; λ_{Water} and λ_{Grain} are the thermal conductivities of pore water and solid grains, respectively; and ϕ is the fractional porosity of the rock sample (e.g., Lin et al., 2011; Pribnow & Sass, 1995; Woodside & Messmer, 1961).

We combined all of the data pairs ($n = 84$) of thermal conductivity and porosity of the sediment core samples and then obtained a linear regression following Equation 3 using least squares analysis (Figure 8b):

$$\ln\left(\lambda_{\text{Bulk}}\right) = -1.09\phi + 0.977, \tag{4}$$

or

$$\lambda_{\text{Bulk}} = \exp(-1.09\phi + 0.977), \tag{5}$$

where λ_{Bulk} is in $\text{Wm}^{-1}\text{K}^{-1}$, ϕ is the dimensionless fractional porosity, and $R^2 = 0.84$. From this regression, we calculate the thermal conductivity of solid grains λ_{Grain} and water λ_{Water} by extrapolation, namely, by setting the porosity to 0 and 1, respectively. The results indicate that $\lambda_{\text{Grain}} = 2.66\ \text{Wm}^{-1}\text{K}^{-1}$ and $\lambda_{\text{Water}} = 0.89\ \text{Wm}^{-1}\text{K}^{-1}$. The calculated λ_{Grain} is almost the same as 2.6 $\text{Wm}^{-1}\text{K}^{-1}$, which is the best value assumed for fitting the experimental thermal conductivity values of Tobin et al. (2015b). The calculated λ_{Water}, however, is larger than the typical seawater value (0.61 $\text{Wm}^{-1}\text{K}^{-1}$ at 25°C and atmospheric pressure; Jamieson & Tudhope, 1970). This difference is probably caused by the extrapolation of the porosity range to 1.0 for the state of water alone which is far away from our tested porosity range from ~0.2 to 0.6. The other possible reason may be that the sediment core samples have different mineral compositions. In contrast, the Equations 4 and 5 assume the thermal conductivity of solid grains are the same for all the samples.

We measured thermal conductivity of sediments under different high effective confining pressures but under a constant pore pressure of 10 MPa (i.e., not the actual in situ pore pressure varying with depth) and a room temperature to simulate the in situ high pressure and high temperature conditions. At the maximum depth of our research target ~3 kmbsf, the pore pressure can be considered as ~50 MPa (~2-km water depth at C0002 site) and ~100°C (Sugihara et al., 2014). El'darov (2003) reported that thermal conductivity of a 3.0 wt% aqueous solution at 10 MPa and 20°C and 50 MPa and 100°C are 0.60 and 0.70 $Wm^{-1}K^{-1}$, respectively. To discuss effects of difference of pressure and temperature of pore water, $\lambda_{Bulk\_(50\ MPa\ \&\ 100°C)}$ / $\lambda_{Bulk\_(10\ MPa\ \&\ 20°C)}$ can be estimated as $[\lambda_{Water\_(50\ MPa\ \&\ 100°C)} / \lambda_{Water\_(10\ MPa\ \&\ 20°C)}]^{\phi}$, according to Equation 2. By assuming fractional porosity at the depth is 0.2, $\lambda_{Bulk\_(50\ MPa\ \&\ 100°C)}$ / $\lambda_{Bulk\_(10\ MPa\ \&\ 20°C)}$ = $(0.70/0.60)^{0.2}$ = 1.03. That is, the influence of pore water pressure and temperature on the sediment thermal conductivity is ~3% increasing.

5. Estimation of Thermal Conductivity in the Accretionary Prism at NanTroSEIZE Drilling Site C0002

The pressure and temperature conditions of both sediments and basement likely change during subduction. An increase of pressure is expected to make soft sediments with high porosity and abundant pore water initially compact/consolidate and significantly decrease their porosity during subduction and/or accretion, which may consequently change their physical properties including thermal conductivity. However, this is not readily testable owing to the very limited number of core samples retrieved from Deep Drilling Site C0002. Consequently, only a few data points have been reported deeper than ~1,100 mbsf with a maximum depth of 3,262.5 mbsf: a few from 2,170–2,215 mbsf in Borehole C0002P and one from 2,836.5–2,848.5 mbsf in Borehole C0002T (Jin et al., 2019; Tobin et al., 2015b). Luckily, porosity was determined by moisture and density (MAD) measurements over almost the whole penetrated depth range using intact handpicked cuttings samples, from which artificial cuttings were excluded and verified by the limited core samples. A reliable porosity depth profile was thus established (Figure 9a after Tobin et al., 2015b, and Kitajima et al., 2017).

Furthermore, a full data set of elastic P wave velocities in Site C0002 from seafloor to 3,058.5 mbsf was obtained from drill logs at different depth intervals in Boreholes C0002A, C0002F, and C0002P (Hamada et al., 2018; Kitajima et al., 2017). The log data indicate that P wave velocity (*Vp*) increases gradually and monotonously with depth to ~2,000 mbsf but remains essentially constant between ~2,200 and ~3,050 mbsf (Figure 9b). Kitajima et al. (2017) used this *Vp* depth profile to estimate the in situ porosity depth profile of sediments at Site C0002 to ~3,050 mbsf based on the following empirical relationship developed by Erickson and Jarrard (1998).

$$Vp = 1.11 + 0.178\phi + 0.305/\left[(\phi+0.135)^2 + 0.0775\right] \\ +0.61\ (V_{sh} - 1)\{\tanh[20(\phi - 0.39)]\text{-}|\tanh[20(\phi - 0.39)]|\}, \quad (6)$$

where *Vp* is in km/s, V_{sh} is shale fraction, and fractional porosity ϕ is dimensionless. The data from Site C0002 are well fit with $V_{sh} = 0.66$ ($R^2 = 0.74$), and this relation is used to determine the in situ ϕ from the *Vp* data, shown as Figure 9c (Kitajima et al., 2017).

As mentioned in section 4, we obtained an empirical relationship (Equation 5) between thermal conductivity and porosity from measurements under high confining and pore pressures using sediment core samples collected from the input site that will ultimately subduct and/or accrete to the accretionary prism. The porosity of the sediment core samples ranges from ~60% to ~20%, which nearly matches the porosity of sediments down to ~3,000 mbsf at Site C0002. The empirical equation can thus be used to estimate the thermal conductivity depth profiles for Site C0002 from porosities both measured by MAD (Figure 9a) and derived from *Vp* (Figure 9c). The results show that the estimated thermal conductivity increases gradually and monotonously with depth, from ~1.3 $Wm^{-1}K^{-1}$ at the seafloor to ~2.2 $Wm^{-1}K^{-1}$ at ~3,050 mbsf (Figure 9d).

In principle, porosities of the core and intact handpicked cuttings samples were measured by MAD at atmospheric pressure, and thermal conductivities estimated from the MAD porosities may therefore represent values under ambient pressure conditions rather than high-pressure conditions. However, the porosities derived from the *Vp* log data are in situ porosities, and the thermal conductivity from the *Vp*-derived porosity may better represent in situ thermal properties than that of core samples under atmospheric pressure conditions. The thermal conductivities estimated from the *Vp*-derived porosities are larger than those from the MAD porosities between ~500 and 2,000 mbsf by approximately 5–10%. Hoffman and Tobin (2004) also reported the *Vp*-derived porosities are smaller than the MAD porosity in the Nankai Trough accretionary prism off Cape Muroto. However, similar thermal conductivities are estimated above ~500 mbsf and

10.1029/2020GC009108

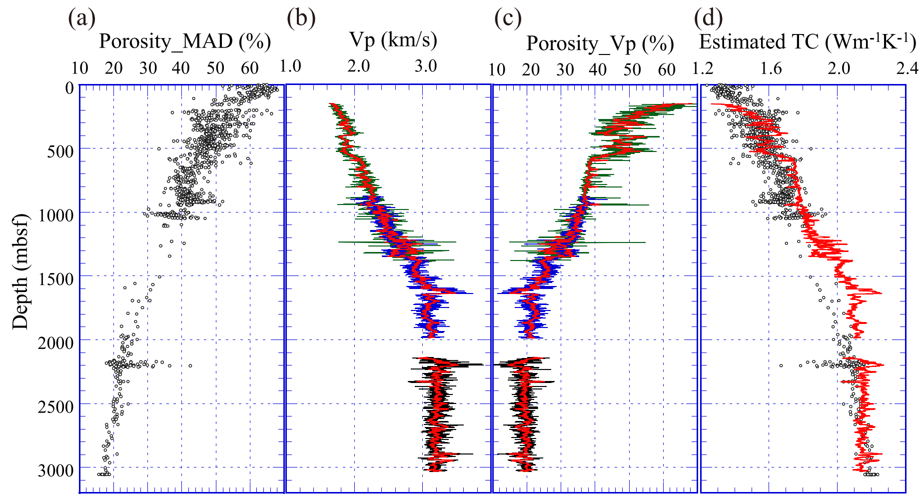

Figure 9. Depth profiles of (a) porosity determined by MAD measurements using core samples and intact handpicked cuttings from Site C0002 after Tobin et al. (2015b). (b) *P* wave velocity *Vp* obtained from Borehole C0002A in green, C0002F in blue, C0002P in black, and a moving average in red after Kitajima et al. (2017). (c) Porosity (%) derived from *Vp* shown in (b) after Kitajima et al. (2017). The colors of the curves mean are the same as (b). (d) Thermal conductivity profiles estimated by Equation 5 using the porosity by MAD measurements (small circles) and porosity derived by the moving average of *Vp* (red curve).

deeper than ~2,000 mbsf. The pressure at depths above ~500 mbsf is smaller, and its effects are not particularly strong; however, below ~2,000 mbsf, the sediments harden and rebound owing to stress relief, and its effects are not significant.

The thermal conductivity measured onboard using core samples from 2,170–2,215 mbsf have a mean and standard deviation of 1.73 ± 0.08 $Wm^{-1}K^{-1}$ (calculated based on all of the individual values in Table T36 of Tobin et al., 2015b), which is within the estimated thermal conductivity range by the MAD porosities in this study but close to the lower boundary. In addition, the wide porosity distribution (~20–40%) at 2,170–2,215 mbsf suggests a significant scattering of physical properties over this depth interval (Figure 9a). The scatter is caused by including porosity data from the fault zone samples. At a depth of ~2,840 mbsf, the measured thermal conductivity of a core sample was reported to be ~2.2 $Wm^{-1}K^{-1}$ (Jin et al., 2019) and showed a similar or slightly larger value than our estimates over the same depth range.

The continuous thermal conductivity depth profile down to ~3 kmbsf estimated in this study is the unique data set in such deep range in an accretionary prism of subduction zones globally. In a shallower depth ranges down to ~1 kmbsf, some comparable data sets are available from ODP and IODP projects and show the same sense in which the thermal conductivity gradually increases with depth, for example, in the Nankai Trough off Cape Muroto (Fisher et al., 1993; Heuer et al., 2017) and in the Costa Rica subduction zone (Hass & Harris, 2016). In the Nankai Trough seismogenic zone, there were several thermal models for estimating the current thermal structure. Hyndman et al. (1995) and Wang et al. (1995) used 2-D isoparametric models to estimate the temperature structure of the sections across Shikoku and across the Kii peninsula. However, these models are unable to account for large observed thermal anomaly (Yamano et al., 2003). As we know, the thermal conductivity profile is not only important but also indispensable in all temperature models. We can obtain more reliable and accurate thermal structure of the Nankai subduction zone with better thermal conductivity profile. Consequently, this work is useful for estimating the depth range of seismogenic regions within the Nankai subduction zone by thermal models with marine heat flow data that is one of the key boundary conditions at the seafloor.

At Site C0002, the in situ temperature has been estimated to increase with depth and reach ~100°C at ~3 kmbsf (Sugihara et al., 2014; Yabe et al., 2019). Indeed, temperature effects on the thermal conductivity of the Nankai sediments should also be examined for estimating in situ thermal conductivity. Lin et al. (2018) reported that thermal conductivity changed less than ~7% over a temperature range between room temperature and 100°C for a basalt core sample taken from the same Site C0012, which suggests that temperature should have a smaller effect on thermal conductivity than pressure. In light of the absence of data regarding the temperature effect of thermal conductivity for oceanic sediments, we do not presently consider the effects of temperature on the in situ thermal conductivity. Nevertheless, we are designing further improvements to our current thermal property measurement system to allow measurements under simultaneously high temperature and high pressure conditions to address these effects on the thermal conductivity of accretionary prism sediments. In addition to the effects of such physical conditions as pressure and temperature and diagenetic and mineralogic actions of cementations, clay mineral transformations under high temperatures (e.g., from smectite to illite and/or from opal to quartz) may also influence physical properties of sediments in greater depths. Examination and evaluation of these geological timescale phenomena may need other approaches rather than our experiments in this study.

6. Conclusions

Knowledge of sediment thermal conductivity is necessary for understanding the thermal structure of active seismogenic zones, such as the Nankai Trough subduction zone, SW Japan. If available, thermal conductivities may be easily determined by laboratory measurements using drill core samples. However, only a very limited number of drill core samples have been collected in the Nankai Trough accretionary prism by the NanTroSEIZE, IODP. Thus, a complete thermal conductivity depth profile in the accretionary prism is not available. The thermal conductivity of water-saturated sediments may depend mainly on their solid grain components and porosity. Based on this consideration, we conducted experiments to determine a quantitative relationship between the thermal conductivity and porosity of the core samples. We used core samples with the same or similar solid grain components as those from the Nankai Trough accretionary prism. Because sediments from sedimentary formations overlaying the incoming subducting oceanic basement will ultimately subduct in the accretionary wedge, they are expected to have the same or similar solid grain components. We therefore collected whole-round sediment core samples obtained from sedimentary formations at the NanTroSEIZE Input Site C0012 and measured their thermal conductivity over a wide range of effective pressures to simulate subduction by changing the sample porosity.

We measured the thermal conductivity of six core samples from a depth range of ~144 to ~518 mbsf at Site C0012 under high-pressure conditions to a maximum effective pressure of ~50 MPa corresponding to a depth of more than ~4 kmbsf. We obtain an empirical equation between thermal conductivity λ_{Bulk} in $\mathrm{Wm}^{-1}\mathrm{K}^{-1}$ and fractional porosity ϕ for the Nankai Trough accretionary prism as $\lambda_{\mathrm{Bulk}} = \exp(-1.09\phi + 0.977)$. Based on porosity data sets from the NanTroSEIZE Centerpiece Site C0002 measured both using core/cuttings samples and derived from *P* wave velocity logs, we estimated complete thermal conductivity profiles down to ~3 kmbsf in the Nankai Trough accretionary prism. In principle, the thermal conductivity estimated from porosities measured using the core/cuttings samples may better represent values under atmospheric pressure conditions and not in situ high-pressure conditions. Porosities derived from the P wave velocity log may better represent the in situ porosities. Nevertheless, the two thermal conductivity profiles show a consistent trend with no significant differences. The profiles also agree with existing thermal conductivity data measured using limited core samples from the accretionary prism.

Data Availability Statement

All thermal conductivity data measured under high pressure (Figures 6–8) and estimated from MAD porosity and *Vp*-derived porosity (Figures 9c and 9d) are available on the Pangaea data publisher for earth and environmental science (https://doi.pangaea.de/10.1594/PANGAEA.918951). Porosity and *Vp* raw data (Figures 9a and 9b) obtained by IODP are available online (http://sio7.jamstec.go.jp/).

Acknowledgments

This study used sediment core samples retrieved from NanTroSEIZE Expeditions 322 and 333 provided by the IODP. Constructive comments from two reviewers, Patrick Fulton and Heinrich Villinger, were very helpful for improving the manuscript. The authors gratefully acknowledge Osamu Matsubayashi for sharing a core sample (C0012G01R4) and Toshiya Kanamatsu, Saneatsu Saito, Masataka Kinoshita, and the other NanTroSEIZE scientists for their helpful discussions. Part of the work was supported by Grants-in-Aid for Scientific Research 16H04065 and 19H00717 of the Japan Society for the Promotion of Science (JSPS), Japan. We thank Esther Posner from Edanz Group for editing a draft of this manuscript.

References

Abdulagatova, Z., Abdulagatov, I. M., & Emirov, V. N. (2009). Effect of temperature and pressure on the thermal conductivity of sandstone. *International Journal of Rock Mechanics and Mining Sciences*, *46*(6), 1055–1071. https://doi.org/10.1016/j.ijrmms.2009.04.011

Ando, M. (1975). Source mechanisms and tectonic significance of historical earthquakes along the Nankai Trough, Japan. *Tectonophysics*, *27*(2), 119–140. https://doi.org/10.1016/0040-1951(75)90102-X

Beardsmore, G. R., & Cull, J. P. (2001). *Crustal heat flow* (p. 324). Cambridge: Cambridge University Press. https://doi.org/10.1017/CBO9780511606021

Byrne, T. B., Lin, W., Tsutsumi, A., Yamamoto, Y., Lewis, J. C., Kanagawa, K., et al. (2009). Anelastic strain recovery reveals extension across SW Japan subduction zone. *Geophysical Research Letters*, *36*, L23310. https://doi.org/10.1029/2009GL040749

El'darov, V. S. (2003). Thermal conductivity of aqueous solutions of KCl–NaCl–$CaCl_2$ system at high temperatures and pressures. *High Temperature*, *41*, 327–331. https://doi.org/10.1023/A:1024282308625

Erickson, S. N., & Jarrard, R. D. (1998). Velocity-porosity relationships for water-saturated siliciclastic sediments. *Journal of Geophysical Research*, *103*(B12), 30,385–30,406. https://doi.org/10.1029/98JB02128

Expedition 322 Scientists (2010a). Site C0012. In Saito, S., Underwood, M.B., Kubo, Y., and the Expedition 322 Scientists, Proc. IODP 322: Tokyo (Integrated Ocean Drilling Program Management International, Inc.). https://doi.org/10.2204/iodp.proc.322.104.2010

Expedition 322 Scientists (2010b). Core description Site C0012. In Saito, S., Underwood, M.B., Kubo, Y., and the Expedition 322 Scientists, Proc. IODP 322: Tokyo (Integrated Ocean Drilling Program Management International, Inc.). Retrieved from http://publications.iodp.org/proceedings/322/EXP_REPT/CORES/CORC0012.PDF

Expedition 333 Scientists (2012a). Expedition 333 summary. In Henry, P., Kanamatsu, T., Moe, K., and the Expedition 333 Scientists, Proc. IODP 333: Tokyo (Integrated Ocean Drilling Program Management International, Inc.). https://doi.org/10.2204/iodp.proc.333.101.2012

Expedition 333 Scientists (2012b). Site C0012. In Henry, P., Kanamatsu, T., Moe, K., and the Expedition 333 Scientists, Proc. IODP 333: Tokyo (Integrated Ocean Drilling Program Management International, Inc.). https://doi.org/10.2204/iodp.proc.333.105.2012

Fisher, A.T., Foucher, J.P., Yamano, M., and Hyndman, R. (1993). Data report: Corrected thermal conductivity data, Leg 131. In: Hill, I.A.; Taira, A.; Firth, J.V. et al. (eds.), *Proceedings of the Ocean Drilling Program, Scientific Results, College Station*, TX (Ocean Drilling Program), 131, 451–456, https://doi.org/10.2973/odp.proc.sr.131.138.1993

Franklin, J. A. Coordinator(1979). Suggest methods for determining water content, porosity, density, absorption and related properties and swelling and slake-durability index properties. *Int. J. Rock Mech. Min. Sci. & Geomech. Abstr*, *16*, 141–156.

Fuchs, S., Schütz, F., Förster, H.-J., & Förster, A. (2013). Evaluation of common mixing models for calculating bulk thermal conductivity of sedimentary rocks: Correction charts and new conversion equations. *Geothermics*, *47*, 40–52. https://doi.org/10.1016/j.geothermics.2013.02.002

Fulton, P. M., Brodsky, E. E., Kano, Y., Mori, J., Chester, F., Ishikawa, T., et al. (2013). Low coseismic friction on the Tohoku-Oki Fault determined from temperature measurements. *Science*, *342*(6163), 1214–1217. https://doi.org/10.1126/science.1243641

Galson, D. P., Wilson, N. P., Schari, U., & Rybach, L. (1987). A comparison of divided-bar and QTM methods of measuring thermal conductivity. *Geothermics*, *16*(3), 215–226. https://doi.org/10.1016/0375-6505(87)90001-0

Hamada, Y., Kitamura, M., Yamada, Y., Sanada, Y., Sugihara, T., Saito, S., et al. (2018). Continuous depth profile of the rock strength in the Nankai accretionary prism based on drilling performance parameters. *Scientific Reports*, *8*(1), 2622. https://doi.org/10.1038/s41598-018-20870-8

Harris, R. N., Schmidt-Schierhorn, F., & Spinelli, G. (2011). Heat flow along the NanTroSEIZE transect: Results from IODP Expeditions 315 and 316 offshore the Kii Peninsula, Japan. *Geochemistry, Geophysics, Geosystems*, *12*, Q0AD16. https://doi.org/10.1029/2011GC003593

Harris, R. N., & Wang, K. (2002). Thermal models of the Middle America Trench at the Nicoya Peninsula, Costa Rica. *Geophysical Research Letters*, *29*, 2010. https://doi.org/10.1029/2002GL015406

Hass, B., & Harris, R. N. (2016). Heat flow along the Costa Rica Seismogenesis Project drilling transect: Implications for hydrothermal and seismic processes. *Geochemistry, Geophysics, Geosystems*, *17*, 2110–2127. https://doi.org/10.1002/2016GC006314

Heki, K., & Miyazaki, S. (2001). Plate convergence and long-term crustal deformation in Central Japan. *Geophysical Research Letters*, *28*(12), 2313–2316. https://doi.org/10.1029/2000GL012537

Heuer, V. B. Inagaki, F., Morono, Y., Kubo, Y., Maeda, L., Bowden, S., et al. (2017). Site C0023. In Heuer, V.B., Inagaki, F., Morono, Y., Kubo, Y., Maeda, L., and the Expedition 370 Scientists. *Temperature limit of the deep biosphere off Muroto* , Proc. IODP 370: College Station, TX (International Ocean discovery program). https://doi.org/10.14379/iodp.proc.370.103.2017

Hoffman, N. W., & Tobin, H. J. (2004). An empirical relationship between velocity and porosity for underthrust sediments in the Nankai Trough accretionary prism. In Mikada, H. et al. (Eds.), *Proc. ODP, Sci. Results* (Vol. 190/196, pp. 1–23). College Station, TX: Ocean Drilling Program. https://doi.org/10.2973/odp.proc.sr.190196.355.2004

Horai, K., & Susaki, J. (1989). The effect of pressure on the thermal conductivity of silicate rocks up to 12 kbar. *Physics of the Earth and Planetary Interiors*, *55*(3-4), 292–305. https://doi.org/10.1016/0031-9201(89)90077-0

Hyndman, R. D., Wang, K., & Yamano, M. (1995). Thermal constraints on the seismogenic portion of the southwestern Japan subduction thrust. *Journal of Geophysical Research*, *100*(B8), 15,373–15,392. https://doi.org/10.1029/95JB00153

Jamieson, D. T., & Tudhope, J. S. (1970). Physical property of sea water solutions: Thermal conductivity. *Desalination*, *8*(3), 393–401. https://doi.org/10.1016/S0011-9164(00)80240-4

Jin, Z., Bedford, J. D., Kitamura, M., Sone, H., Stanislowski, K., Hamada, Y., et al. (2019). *Physical properties of the Nankai Trough at Sites C0002, C0024 and C0025, IODP Expedition 358, Paper T51G-0365 presented at 2019 Fall Meeting*. San Francisco, CA: American Geophysical Union.

Kanamori, H. (1972). Tectonic implications of the 1944 Tonankai and the 1946 Nankaido earthquakes. *Physics of the Earth and Planetary Interiors*, *5*, 129–139. https://doi.org/10.1016/0031-9201(72)90082-9

Kinoshita, M., Moore, G., von Huene, R., Tobin, H., & Ranero, C. (2006). The seismogenic zone experiment. *Oceangraph*, *19*(4), 28–38. https://doi.org/10.5670/oceanog.2006.02

Kitajima, H., Saffer, D., Sone, H., Tobin, H., & Hirose, T. (2017). In situ stress and pore pressure in the deep interior of the Nankai accretionary prism, Integrated Ocean Drilling Program Site C0002. *Geophysical Research Letters*, *44*, 9644–9652. https://doi.org/10.1002/2017GL075127

Kukkonen, I. T., Jokinen, J., & Seipold, U. (1999). Temperature and pressure dependencies of thermal transport properties of rocks: Implications for uncertainties in thermal lithosphere models and new laboratory measurements of high-grade rocks in the central Fennoscandian shield. *Surveys in Geophysics*, *20*(1), 33–59. https://doi.org/10.1023/A:1006655023894

Lin, W., Byrne, T., Kinoshita, M., McNeill, L., Chang, C., Lewis, J., et al. (2016). Distribution of stress state in the Nankai subduction zone, southwest Japan and a comparison with Japan Trench. *Tectonophysics*, *692*, 120–130. https://doi.org/10.1016/j.tecto.2015.05.008

Lin, W., Fulton, P. M., Harris, R. N., Tadai, O., Matsubayashi, O., Tanikawa, W., & Kinoshita, M. (2014). Thermal conductivities, thermal diffusivities, and volumetric heat capacities of core samples obtained from the Japan Trench Fast Drilling Project (JFAST). *Earth, Planets and Space*, *66*(1), 48. https://doi.org/10.1186/1880-5981-66-48

Lin, W., Tadai, O., Hirose, T., Tanikawa, W., Takahashi, M., Mukoyoshi, H., & Kinoshita, M. (2011). Thermal conductivities under high pressure in core samples from IODP NanTroSEIZE drilling site C0001. *Geochemistry, Geophysics, Geosystems*, *12*, Q0AD14. https://doi.org/10.1029/2010GC003449

Lin, W., Tadai, O., Kinoshita, M., Kameda, J., Tanikawa, W., Hirose, T., et al. (2018). Thermal conductivity changes in subducting basalt, Nankai subduction zone, SW Japan: An estimation from laboratory measurements under separate high-pressure and high-temperature conditions. In Byrne, T. et al. (Eds.), *Geology and Tectonics of Subduction Zones: A Tribute to Gaku Kimura* (Vol. 534, pp. 35–50). Boulder, CO: Geological Society of America Special Paper. https://doi.org/10.1130/2018.2534(02)

Miyazaki, S., & Heki, K. (2001). Crustal velocity field of southwest Japan: Subduction and arc-arc collision. *Journal of Geophysical Research*, *106*(B3), 4305–4326. http://doi.org/10.1029/2000JB900312

Mizutani, T., Hirauchi, K.-I., Lin, W., & Sawai, M. (2017). Depth dependence of the frictional behavior of montmorillonite fault gouge: Implications for seismicity along a décollement zone. *Geophysical Research Letters*, *44*, 5383–5390. https://doi.org/10.1002/2017GL073465

Morin, R., & Silva, A. J. (1984). The effects of high pressure and high temperature on some physical properties of ocean sediments. *Journal of Geophysical Research*, *89*(B1), 511–526. https://doi.org/10.1029/JB089iB01p00511

Oohashi, K., Lin, W., Wu, H.-Y., Yamaguchi, A., & Yamamoto, Y. (2017). Stress state in the Kumano Basin and in slope sediment determined from anelastic strain recovery: Results from IODP Expedition 338 to the Nankai Trough. *Geochemistry, Geophysics, Geosystems*, *18*, 3608–3616. https://doi.org/10.1002/2017GC007137

Osako, K., Ito, E., & Yoneda, A. (2004). Simultaneous measurements of thermal conductivity and thermal diffusivity for garnet and olivine under high pressure. *Physics of the Earth and Planetary Interiors*, *143-144*, 311–320. https://doi.org/10.1016/j.pepi.2003.10.010

Park, J.-O., Tsuru, T., Kodaira, S., Cummins, P. R., & Kaneda, Y. (2002). Splay fault branching along the Nankai subduction zone. *Science*, *297*(5584), 1157–1160. https://doi.org/10.1126/science.1074111

Pribnow, D., & Sass, J. H. (1995). Determination of thermal conductivity from deep boreholes. *Journal of Geophysical Research*, *100*(B6), 9981–9994. https://doi.org/10.1029/95JB00960

Pribnow, D., Williams, C. F., Sass, J. H., & Keating, R. (1996). Thermal conductivity of water-saturated rocks from the KTB pilot hole at temperature of 25 to 300 °C. *Geophysical Research Letters*, *23*(4), 391–394. https://doi.org/10.1029/95GL00253

Saito, S., Underwood, M. B., & Kubo, Y. (2009). NanTroSEIZE Stage 2: Subduction inputs. *IODP Sci. Prosp*, 322, Tokyo: Integrated Ocean Drilling Program Management International, Inc. https://doi.org/10.2204/iodp.sp.322.2009

Sass, J. H., Stone, C., & Munroe, R. J. (1984). Thermal conductivity determinations on solid rock—A comparison between a steady-state divided bar apparatus and a commercial transient line-source device. *Journal of Volcanology and Geothermal Research*, *20*(1-2), 145–153. https://doi.org/10.1016/0377-0273(84)90071-4

Scholz, C. H. (1998). Earthquakes and friction laws. *Nature*, *391*(6662), 37–42. https://doi.org/10.1038/34097

Seipold, U., & Huenges, E. (1998). Thermal properties of gneisses and amphibolites high pressure and high temperature investigations of KTB-rock samples. *Tectonophysics*, *291*(1-4), 173–178. https://doi.org/10.1016/S0040-1951(98)00038-9

Seno, T., Stein, S., & Gripp, A. E. (1993). A model for the motion of the Philippine Sea plate consistent with NUVEL-1 and geological data. *Journal of Geophysical Research*, *98*(B10), 17,941–17,948. https://doi.org/10.1029/93JB00782

Spinelli, G. A. (2014). Long-distance fluid and heat transport in the oceanic crust entering the Nankai subduction zone, NanTroSEIZE transect. *Earth and Planetary Science Letters*, *389*, 86–94. https://doi.org/10.1016/j.epsl.2013.12.013

Stesky, R. M., Brace, W. F., Riley, D. K., & Robin, P.-Y. F. (1974). Friction in faulted rock at high temperature and pressure. *Tectonophysics*, *23*(1-2), 177–203. https://doi.org/10.1016/0040-1951(74)90119-X

Sugihara, T., Kinoshita, M., Araki, E., Kimura, T., Kyo, M., Namba, Y., et al. (2014). Re-evaluation of temperature at the updip limit of locked portion of Nankai megasplay inferred from IODP Site C0002 temperature observatory. *Earth, Planets and Space*, *66*, 107. https://doi.org/10.1186/1880-5981-66-107

Tanikawa, W., Hirose, T., Mukoyoshi, H., Tadai, O., & Lin, W. (2013). Fluid transport properties in sediments and their role in large slip near the surface of the plate boundary fault in the Japan Trench. *Earth and Planetary Science Letters*, *382*, 150–160. https://doi.org/10.1016/j.epsl.2013.08.052

Tanikawa, W., Tadai, O., Morita, S., Lin, W., Yamada, Y., Sanada, Y., et al. (2016). Thermal properties and thermal structure in the deep-water coalbed basin off the Shimokita Peninsula. *Japan, Marine and Petroleum Geology*, *73*, 445–461. https://doi.org/10.1016/j.marpetgeo.2016.03.006

Tobin, H., Hirose, T., Ikari, M., Kanagawa, K., Kimura, G., Kinoshita, M., et al. (2019). Expedition 358 Preliminary Report: NanTroSEIZE Plate Boundary Deep Riser 4: Nankai seismogenic/slow slip megathrust. International Ocean Discovery Program. https://doi.org/10.14379/iodp.pr.358.2019

Tobin, H., Hirose, T., Saffer, D., Toczko, S., Maeda, L., Kubo, Y., et al. (2015a). Expedition 348 summary. In Tobin, H., Hirose, T., Saffer, D., Toczko, S., Maeda, L., Kubo, Y., and the Expedition 348 Scientists, *Proc. IODP, 348: College Station*, TX (Integrated Ocean Drilling Program). https://doi.org/10.2204/iodp.proc.348.101.2015

Tobin, H., Hirose, T., Saffer, D., Toczko, S., Maeda, L., Kubo, Y., et al. (2015b). Site C0002. In H. Tobin, T. Hirose, D. Saffer, S. Toczko, L. Maeda, Y. Kubo, & the Expedition 348 Scientists (Eds.), *Proc. IODP, 348: College Station*. TX: Integrated Ocean Drilling Program. https://doi.org/10.2204/iodp.proc.348.103.2015

Tobin, H. J., Kimura, G., & Kodaira, S. (2019). Processes governing giant subduction earthquakes: IODP drilling to sample and instrument subduction zone megathrusts, *Oceanography*, *32*, No.1, Special Issue on Scientific Ocean Drilling: Looking to the Future, 80-93.

Tobin, H. J., & Kinoshita, M. (2006). Investigations of seismogenesis at the Nankai Trough, Japan. IODP Sci. Prosp. NanTroSEIZE Stage 1. https://doi.org/10.2204/iodp.sp.nantroseize1.2006

Underwood, M. B., Saito, S., Kubo, Y., & the Expedition 322 Scientists (2010). Expedition 322 summary. In Saito, S., Underwood, M.B., Kubo, Y., and the Expedition 322 Scientists, Proc. IODP, 322: Tokyo (Integrated Ocean Drilling Program Management International, Inc.). https://doi.org/10.2204/iodp.proc.322.101.2010

Wang, K., Hyndman, R. D., & Yamano, M. (1995). Thermal regime of the Southwest Japan subduction zone: Effects of age history of the subducting plate. *Tectonophysics*, *248*(1-2), 53–69. https://doi.org/10.1016/0040-1951(95)00028-L

Woodside, W., & Messmer, J. H. (1961). Thermal conductivity of porous media. I. Unconsolidated sands. *Journal of Applied Physics*, *32*(9), 1688–1688. https://doi.org/10.1063/1.1728419

Xu, Y., Shankland, T. J., Linhardt, S., Rubie, D. C., Langenhorst, F., & Klasinski, K. (2004). Thermal diffusivity and conductivity of olivine, wadsleyyite and ringwoodite to 20 GPa and 1373 K. *Physics of the Earth and Planetary Interiors*, *143-144*, 321–336. https://doi.org/10.1016/j.pepi.2004.03.005

Yabe, S., Fukuchi, R., Hamada, Y., & Kimura, G. (2019). Simultaneous estimation of in situ porosity and thermal structure from core sample measurements and resistivity log data at Nankai accretionary prism. *Earth, Planets and Space*, *71*, 116. https://doi.org/10.1186/s40623-019-1097-4

Yamamoto, Y., Lin, W., Oda, H., Byrne, T., & Yamamoto, Y. (2013). Stress states at the subduction input site, Nankai Subduction Zone, using anelastic strain recovery (ASR) data in the basement basalt and overlying sediments. *Tectonophysics*, *600*, 91–98. https://doi.org/10.1016/j.tecto.2013.01.028

Yamano, M., Kinoshita, M., Goto, S., & Matsubayashi, O. (2003). Extremely high heat flow anomaly in the middle part of the Nankai Trough. *Physics and Chemistry of the Earth*, *28*(9-11), 487–497. https://doi.org/10.1016/S1474-7065(03)00068-8